Monthly Notices
of the
ROYAL ASTRONOMICAL SOCIETY

MNRAS **493,** L132–L137 (2020)
Advance Access publication 2020 February 6

doi:10.1093/mnrasl/slaa019

Radio and X-ray detections of GX 339–4 in quiescence using MeerKAT and *Swift*

E. Tremou,[1★] S. Corbel,[1,2★] R. P. Fender,[3,4] P. A. Woudt,[4] J. C. A. Miller-Jones,[5] S. E. Motta,[3] I. Heywood,[3,6] R. P. Armstrong,[3,4,7] P. Groot,[4,8,9] A. Horesh,[10] A. J. van der Horst,[11,12] E. Koerding,[9] K. P. Mooley,[13,14,15] A. Rowlinson[16,17] and R. A. M. J. Wijers[16]

[1]*AIM/CEA Paris-Saclay, Université Paris Diderot, CNRS, F-91191 Gif-sur-Yvette, France*
[2]*Station de Radioastronomie de Nançay, Observatoire de Paris, PSL Research University, CNRS, Univ. Orléans, F-18330 Nançay, France*
[3]*Astrophysics, Department of Physics, University of Oxford, Keble Road, Oxford OX1 3RH, UK*
[4]*Inter-University Institute for Data-Intensive Astronomy, Department of Astronomy, University of Cape Town, Private Bag X3, Rondebosch 7701, South Africa*
[5]*International Centre for Radio Astronomy Research, Curtin University, GPO Box U1987, Perth, WA 6845, Australia*
[6]*Department of Physics and Electronics, Rhodes University, PO Box 94, Grahamstown 6140, South Africa*
[7]*South African Radio Astronomy Observatory, 2 Fir Street, Black River Park, Observatory, Cape Town 7925, South Africa*
[8]*South African Astronomical Observatory, PO Box 9, Observatory, Cape Town 7935, South Africa*
[9]*Department of Astrophysics/IMAPP, Radboud University Nijmegen, PO Box 9010, NL-6500 GL Nijmegen, the Netherlands*
[10]*Racah Institute of Physics, The Hebrew University of Jerusalem, Jerusalem 91904, Israel*
[11]*Department of Physics, The George Washington University, 725 21st Street NW, Washington, DC 20052, USA*
[12]*Astronomy, Physics and Statistics Institute of Sciences (APSIS), 725 21st Street NW, Washington, DC 20052, USA*
[13]*Department of Physics, University of Oxford, Keble Road, Oxford OX1 3RH, UK*
[14]*National Radio Astronomy Observatory, Socorro, NM 87801, USA*
[15]*Caltech, 1200 E. California Blvd. MC 249-17, Pasadena, CA 91125, USA*
[16]*Anton Pannekoek Institute, University of Amsterdam, Postbus 94249, NL-1090 GE Amsterdam, the Netherlands*
[17]*Netherlands Institute for Radio Astronomy (ASTRON), Oude Hoogeveensedijk 4, NL-7991 PD Dwingeloo, the Netherlands*

Accepted 2020 February 3. Received 2020 January 17; in original form 2019 December 5

ABSTRACT

The radio–X-ray correlation that characterizes accreting black holes at all mass scales – from stellar mass black holes in binary systems to supermassive black holes powering active galactic nuclei – is one of the most important pieces of observational evidence supporting the existence of a connection between the accretion process and the generation of collimated outflows – or jets – in accreting systems. Although recent studies suggest that the correlation extends down to low luminosities, only a handful of stellar mass black holes have been clearly detected, and in general only upper limits (especially at radio wavelengths) can be obtained during quiescence. We recently obtained detections of the black hole X-ray binary (XRB) GX 339–4 in quiescence using the Meer Karoo Array Telescope (MeerKAT) radio telescope and *Swift* X-ray Telescope instrument on board the *Neil Gehrels Swift Observatory*, probing the lower end of the radio–X-ray correlation. We present the properties of accretion and of the connected generation of jets in the poorly studied low-accretion rate regime for this canonical black hole XRB system.

Key words: radio continuum: transients – X-rays: binaries.

1 INTRODUCTION

X-ray binaries (XRBs) are binary systems composed of a compact stellar remnant (a black hole or a neutron star) and a companion star with active mass accretion on to the stellar remnant. The presence of the collapsed star is revealed by X-ray and radio activity whose (relative and absolute) strength depends on the accretion rate on to the compact object and the state of the accretion disc that forms around the compact object. In low-mass XRBs, the accretion from a low-mass donor star occurs through Roche lobe overflow: matter streams from the companion star to the compact one, forming an accretion disc that redistributes angular momentum and emits copious radiation peaking in the X-rays.

★ E-mail: evangelia.tremou@cea.fr (ET), stephane.corbel@cea.fr (SC)

Transient XRBs spend most of their lives in a so-called *quiescent state*, during which they accrete at very low mass-accretion rates and emit at X-ray luminosities ranging between 10^{30} and 10^{33} erg s^{-1} (Kong et al. 2002; Gallo et al. 2008). The quiescent state is interrupted by occasional *outbursts*, active phases that can last from weeks to years, during which the source's X-ray luminosity can reach or even cross the Eddington limit, $L_{\rm Edd}$ (King 2000). The accretion rate and luminosity of XRBs, and their X-ray spectral and fast time-variability properties, change dramatically as they go through the quiescence/outburst cycle (Remillard & McClintock 2006).

While an optically thick, geometrically thin accretion disc (thermal emission) dominates the X-ray emission at high accretion rates, non-thermal radiation from a radiatively inefficient accretion flow located in the inner regions of the accretion disc dominates at lower rates (Yuan & Narayan 2014). The radiatively inefficient accretion flow is believed to be linked to the generation of compact jets, which emit synchrotron radiation, with a peak luminosity in the radio regime (Corbel et al. 2000; Fender 2001). Such jets appear to dominate the energetics of the system at low accretion rates (Fender, Gallo & Jonker 2003), and may even be responsible for part of the X-ray emission (Markoff et al. 2003; Markoff & Nowak 2004) during the hard states. As a consequence, the radio and X-ray emission at low accretion rates are tightly correlated (e.g. Hannikainen et al. 1998; Corbel et al. 2000, 2003, 2013; Gallo, Fender & Pooley 2003b; Coriat et al. 2011; Gallo, Miller & Fender 2012; Gallo et al. 2014; Tetarenko et al. 2016), and the radio–X-ray correlation is one of the most important pieces of observational evidence supporting the existence of a correlation between accretion and the generation of jets, also called *disc–jet coupling*. This correlation encompasses accreting compact objects at all scales (thus including supermassive black holes in active galactic nuclei, AGN), when a mass term is considered, and is often referred to as *the Fundamental Plane of activity of black holes* (Merloni, Heinz & di Matteo 2003; Falcke, Körding & Markoff 2004).

While the outburst phases of black hole XRBs are relatively well studied, this is not true for quiescence and the low-luminosity states in general, which are seldom probed due to the difficulties in observing simultaneously these sources at very low fluxes. During such states, one has the opportunity to study the accretion process and the accretion-powered jets in a regime where the thermal emission from the thin disc does not outshine the radiation from non-thermal processes, which might have a fundamental role in the disc–jet coupling. Also, it has been recently shown that the quiescent state can show significant variability (e.g. Miller-Jones et al. 2008; Hynes et al. 2009; Froning et al. 2011; Wu et al. 2016; Plotkin et al. 2019).

Interestingly, differences in the quiescent emission of neutron star versus black hole transients have been proposed as a possible signature of the absence of a hard surface, and might thus provide an indirect evidence for the existence of an event horizon (e.g. Menou et al. 1999; Quataert & Narayan 1999; McClintock et al. 2003, although see Jonker et al. 2006 for difficulties with this interpretation). Hence, studying XRBs at low accretion rates is key to determine what properties – if any – of the disc–jet coupling depend on the nature of the compact object powering these systems.

GX 339–4 is a Galactic XRB with a low-mass companion ($\sim$1 M$_\odot$) orbiting a central black hole with mass $\geq$5.8 M$_\odot$ (Hynes et al. 2004), with an orbital period of 42 h, located at a distance of 8–12 kpc (Zdziarski, Ziółkowski & Mikołajewska 2019). GX 339–4 is one of the best studied black hole X-ray transients, having been observed in the radio and X-rays during several different outbursts over more than 40 yr. GX 339–4 is also one of the key sources in the radio–X-ray correlation, as it is currently the system featuring the best simultaneous X-ray and radio data sets covering several outbursts (Corbel et al. 2013). Here we present only the detection in quiescence.

2 OBSERVATIONS

As part of the large survey project ThunderKAT (Fender et al. 2017), we are studying a large number of radio transients, including many XRBs, in the image domain. The field of the XRB GX 339–4 is observed weekly since 2018 September with the full Meer Karoo Array Telescope (MeerKAT; Jonas 2009) array. A dedicated *Neil Gehrels Swift Observatory* (hereafter referred to as *Swift*; Gehrels et al. 2004) monitoring programme supports these observations, providing weekly X-ray measurements.

2.1 MeerKAT radio observations

The observations discussed here were taken between 2018 April, when the first ThunderKAT data were obtained using the full MeerKAT array, and 2018 November, when the quiescent phase of the source ended with an outburst. The MeerKAT radio telescope is located in the Karoo desert in South Africa and comprises 64 antennas, 13.5 m diameter each, with a maximum baseline of 8 km. Observations were made using the L-band (900–1670 MHz) receiver, split into 4096 frequency channels spanning 856 MHz centred at 1284 MHz. Observations typically alternated between the target and phase calibrator, while a bandpass and flux calibrator were observed at the beginning of the observing block. All observations were obtained in full polarization mode. The data were calibrated following the standard procedures with the Common Astronomy Software Application (CASA; McMullin et al. 2007). Imaging, self-calibration, and direction-dependent calibration of the data were carried out with the new wide-band, wide-field imager, DDFACET (Tasse et al. 2018). For details, see section 2 in Driessen et al. (2020).

2.2 *Swift* X-ray observations

With the aim of studying the X-ray and radio correlation, we used available data taken by the *Swift* X-ray Telescope (XRT) instrument (Burrows et al. 2000). For our analysis, we include measurements made from 2018 September to 2018 November where the source was in the quiescent state. We used eight observations from XRT in photon-counting (PC) mode that are close in time to our radio observations. The counts range between 4 and 17 per observation. Photon pile-up is negligible with such low photon count rates.

We used the output of the standard pipeline processing and we analysed the data using the XSPEC software package (Arnaud 1996). We fit the energy spectra with a power-law model accounting for interstellar absorption, and we applied Cash statistics to obtain the X-ray flux from the combined and the individual spectra. We fixed the column density to $N_{\rm H} = 6 \times 10^{21}$ cm^{-2} (Zdziarski et al. 2004; Cadolle Bel et al. 2011; Corbel et al. 2013) to obtain reliable fit and to constrain the flux and the photon index Γ for the combined spectra. The resulted photon index $\Gamma = 2.2$ was additionally fixed for the individual spectra fits. All measurement IDs and the obtained fluxes are presented in Table 1.

Table 1. MeerKAT and *Swift* observations of GX 339–4.

MJD	Image rms (μJy beam^{-1})	Measured flux (μJy beam^{-1})	Flux 3–9 keV ($\times 10^{-13}$ erg cm^{-2} s^{-1})	Exposure time (ks)	Counts
58222	18.6	51.2	–	–	–
58369	40.1	63.6	–	–	–
58370	–	–	1.29 ± 0.13	1.1	4
58375	26.2	13.2	–	–	–
58382	26.2	40.2	1.38 ± 0.14	2.1	10
58389	35.3	71.6	3.35 ± 0.33	1.9	10
58396	27.7	43.1	3.76 ± 0.38	1.8	16
58402	27.5	82.2	–	–	–
58403	44.8	47.8	3.0 ± 0.3	1.8	17
58410	28.2	17.2	0.83 ± 0.083	1.6	4
58417	–	–	1.52 ± 0.15	2.2	9
58418	25.9	63.4	–	–	–
58423	–	–	8.26 ± 0.83	2.0	9
58425	27.3	74.2	–	–	–
58432	26.5	92.1	–	–	–
58439	32.3	76.2	–	–	–

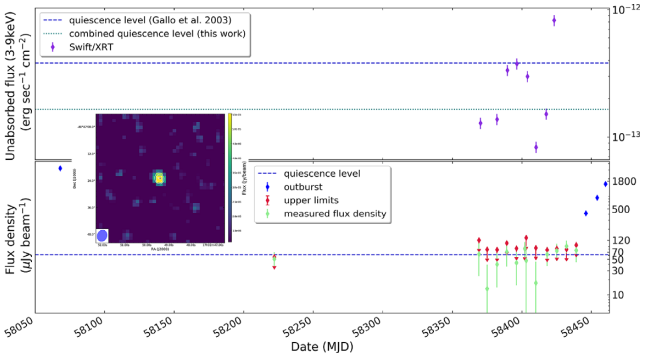

Figure 1. The MeerKAT image showing the detection of GX 339–4 in quiescence and the light curves during the quiescent state. The lower panel shows the radio light curve from MeerKAT observations with red arrows indicating the upper limits, while the green points correspond to the measured flux during this state. The blue dashed line shows the quiescent level. The blue points show the preceding and following outburst phase (Tremou et al. 2018, full outburst will be discussed in a separate study). In the upper panel, the blue line denotes the low-luminosity state as measured by *Chandra* (Gallo, Fender & Corbel 2003a), and the cyan line corresponds to the flux as measured by the combined *Swift*/XRT spectra of the observations shown in Table 1.

3 RESULTS

3.1 Detection in quiescence

We started a weekly monitoring of the black hole XRB GX 339–4 at the end of its 2018 outburst. We obtained in total 13 epochs of the GX 339–4 field with MeerKAT (Table 1). The source was not detected in any of the individual epochs due to its low flux density. We concatenated the individual epochs in the *uv*-plane, and we obtained an image with an rms background noise level of 11 μJy beam^{-1}. Owing to the MeerKAT sensitivity and the visibility stacking technique, we obtained a solid detection of the source at 62 μJy beam^{-1} during its quiescent state by combining 13 epochs, for a total integration time of ∼5 h (Fig. 1).

Fig. 1 shows the 3σ upper limits in red of the individual MeerKAT observations, while in the blue dashed line, we plot the detection level of the stacked image. In the top panel, we plot the fluxes that were obtained from the quasi-simultaneous observations with the *Swift*/XRT instrument (3–9 keV). The source was also detected in the (3–9 keV) individual XRT images. Thanks to the high sensitivity that characterizes the MeerKAT radio telescope and the *Swift* observations, we extend the radio–X-ray correlation for GX 339–4 down to $L_X \sim 10^{-13}$ erg cm^{-2} s^{-1}, thus fully covering this system's evolution cycle.

We have also checked whether the detection in quiescence is dominated by the observations close to the new outburst that started at the end of 2018 November (MJD 58446) (Fig. 1). Therefore, in the combined images, we also excluded the brightest X-ray detection (MJD 58423). The result remained unchanged even without including this observation for the *Swift* image. The same test was performed for the MeerKAT radio map by excluding observing epochs close to the quick rise of the 2018 outburst (Tremou et al. 2018). In particular, we performed a stacking analysis with MeerKAT data by excluding the last three epochs (MJD 58425, 58432, and 58439), where GX 339–4 was detected at the level of ∼57 μJy (∼4.2σ) neglecting the last three epochs.

Furthermore, we searched for radio variability hints on ∼1 month time-scale combining some of the epochs (MJD: 58369–58389, 58396–58418, and 58423–58439), where the signal-to-noise ratio (S/N) allows 3σ detection of the source. The radio variability searches resulted in non-significant change of the flux density above 1σ of the average flux.

The concatenated image was deconvolved over four frequency chunks and hence we were able to obtain a frequency cube that allowed us to measure the flux at each frequency and consequently calculate the spectral index of GX 339–4. The four frequency chunks were centred at 962.9 MHz, 1.17, 1.39, and 1.6 GHz and the flux densities that we obtained were 101.3 ± 3, 84.9 ± 5, 75.4 ± 5, and 57.0 ± 8 μJy beam^{-1} , respectively. This results in a negative spectral index $\alpha \sim -0.8 \pm 0.4$ in contrast to the constantly flat spectra ($\alpha \sim 0.35$) that we see during the 2018–2019 outburst (Tremou et al. in preparation) and in the past hard states (Corbel et al. 2000, 2003, 2013; Fender 2001). Nevertheless, we note here that the subband calibration has not been properly evaluated and hence we are aware that our estimates may include a few per cent of calibration error.

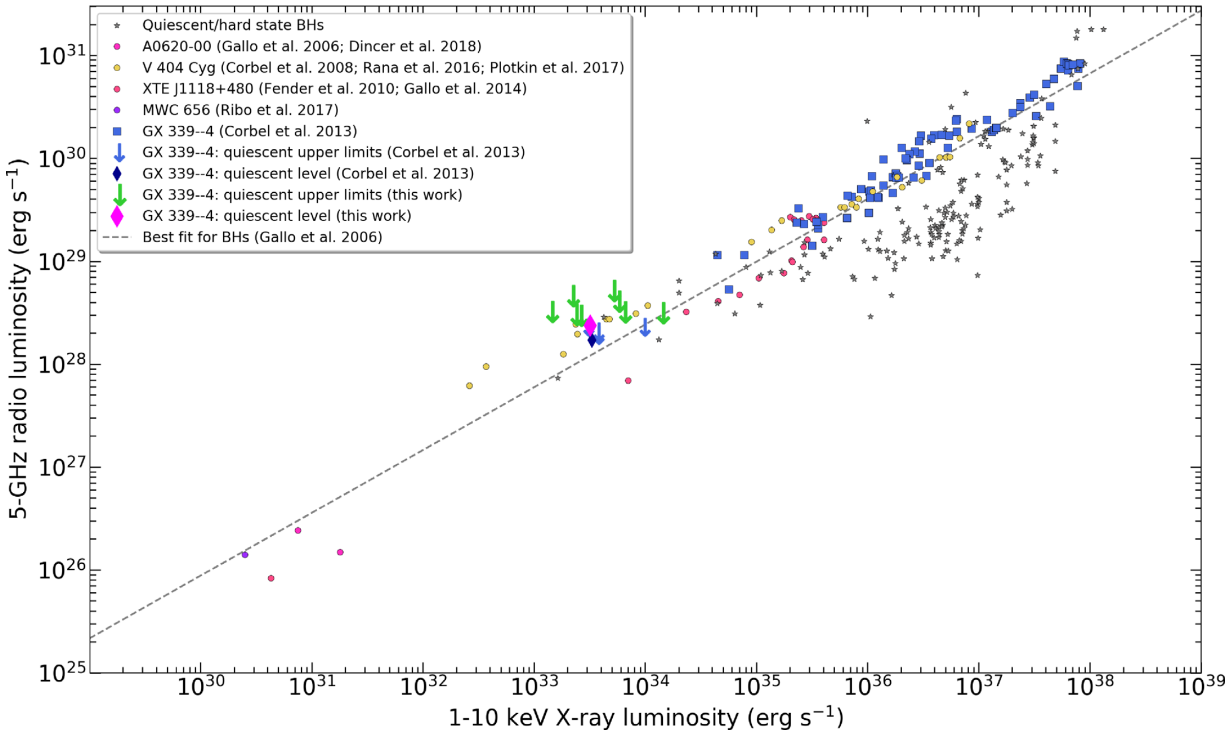

Figure 2. The L_X–L_R correlation of quiescent/hard state black holes in grey using the data base by Bahramian et al. (2018). GX 339–4 is shown in blue squares (outburst) and blue arrows (upper limits) from Corbel et al. (2013). The individual simultaneous measurements of MeerKAT and *Swift*/XRT of this study are shown in green arrows and in purple (diamond), we show the detection in the quiescent state. The blue one denotes the quiescence level from the deep study that has been presented in Corbel et al. (2013), while the grey dashed line corresponds to their fit with a function of the form $L_R \propto L_X^{0.61\pm0.01}$. Quiescent black holes, A0620−00 (Gallo et al. 2006; Dinçer et al. 2018), V404 Cyg (Corbel et al. 2008; Rana et al. 2016; Plotkin et al. 2017), XTE JJ1118+480 (Fender et al. 2010; Gallo et al. 2014) and MWC 656 (Ribó et al. 2017), that have been detected are also overplotted in circles.

3.2 Radio–X-ray correlation

Simultaneous radio and X-ray observations of black hole XRBs in quiescence have successfully detected the targeted sources only for three low-mass XRBs, namely V404 Cyg (Gallo, Fender & Hynes 2005; Hynes et al. 2009), A0620−00 (Gallo et al. 2006), and XTE J1118+480 (Gallo et al. 2014). They revealed a ratio of $L_X/L_{Edd} \leq 10^{-8.5}$, while one high-mass XRB, MWC 656 (Ribó et al. 2017), shows a ratio of $L_X/L_{Edd} \sim 10^{-9}$. Past deep Australia Telescope Compact Array (ATCA; Frater, Brooks & Whiteoak 1992) observations revealed only a marginal detection of GX 339–4 at 5 GHz with a flux density of 73 ± 16 μJy showing a negative spectral index, $\alpha = -0.6$ (Corbel et al. 2013). Our current measurements are consistent with the values from Corbel et al. (2013), denoting the true level in quiescence. Although the radio–X-ray correlation seems to continue even in the quiescent state (Plotkin et al. 2017), some hints of changes in the nature of the X-ray emission have been observed at low luminosities ($L_X/L_{Edd} \leq 10^{-5}$; Gallo et al. 2007; Plotkin et al. 2015). Observations at very low accretion rates are therefore key to determine the properties of the faint jets observed in these regimes, and to constrain the still poorly understood physical processes underlying their generation.

In Fig. 2, we place our quasi-simultaneous radio and X-ray measurements from this study on the L_X–L_R plane. In order to compare our results with the population of the quiescent/hard state black holes, we convert the MeerKAT radio flux into radio luminosity at 5 GHz, assuming a distance of 8 kpc and a flat spectral index for consistency with objects at hard state. Assuming the same distance, we used the *Swift*/XRT spectra fitting to obtain the unabsorbed X-ray flux (1–10 keV) and we converted it into X-ray luminosity (1–10 keV). Our data points (green and purple) probe the lower part of the correlation, while the blue and orange points show the previous extensive study of GX 339–4 during its past outburst–quiescence cycles (Corbel et al. 2013). Green arrows show the upper limits obtained by every individual observation reported in this work, while the purple point indicates the level that we obtain from the concatenated image from MeerKAT in radio and *Swift*/XRT in X-rays. The grey dashed line represents the best fit for black holes with a function $L_R \propto L_X^{0.61\pm0.01}$ (Gallo et al. 2006), which is consistent with the fit from the GX 339–4 data presented in Corbel et al. (2013) using a higher radio frequency (9 GHz) than the one presented in this work (1.28 GHz). However, in the case of a flat radio spectrum the results do not vary.

4 DISCUSSION AND CONCLUSIONS

We have presented an X-ray and a radio analysis of the black hole XRB GX 339–4 in quiescence using observations from *Swift*/XRT and MeerKAT. The source was detected during this state in both X-rays and radio. In order to improve our sensitivity, we concatenated data from several epochs from *Swift*/XRT and from MeerKAT, and we detected the source at the level of 1.6×10^{13} erg cm^{-2} s^{-1} and 62 μJy beam^{-1}, respectively.

Sampling the low-luminosity end of the radio–X-ray correlation, we probe low Eddington accretion rates of XRBs at the low X-ray luminosity quiescent level of the order of 10^{33} erg s^{-1}. The radio–X-ray correlation of $L_X \propto L_R^{0.62\pm0.01}$ in GX 339–4 has been

well constrained for the brightest hard states by Corbel et al. (2013) using measurements covering ∼15 yr. Our measurements confirm that the same correlation seems to continue with no break down to low luminosities, where we detect GX 339–4, which is characterized by a soft X-ray spectrum. While the binary system is going towards quiescence from the hard state, the X-ray spectral shape becomes softer until it reaches a constant shape ($\Gamma \sim 2.1$; Corbel, Tomsick & Kaaret 2006; Corbel, Koerding & Kaaret 2008; Plotkin, Gallo & Jonker 2013; Plotkin et al. 2017). Our fitting of the combined *Swift*/XRT spectrum constrains the photon index Γ value that is consistent with the soft X-ray spectra. The soft X-ray spectra favour a mechanism where in the inner regions of the accretion disc, radiatively inefficient outflows are likely to develop within a geometrically thick and hot area.

The slope of the radio–X-ray correlation for GX 339–4 is similar to that of the well-studied binary source V404 Cyg, which has not shown any evidence that a synchrotron cooled jet could dominate the X-ray emission (Plotkin et al. 2017). On the other hand, synchrotron self-Compton (SSC) processes from a radiatively cooled jet or a hot accretion flow may be responsible for generating the X-ray emission (Poutanen & Veledina 2014; Malzac 2016). Furthermore, the X-ray emission in quiescence can be driven by a less efficient particle acceleration along the jet axis implying optically thin synchrotron emission by non-thermal particles (Plotkin et al. 2013; Connors et al. 2017).

MeerKAT radio observations show a negative spectral index $\alpha = -0.8 \pm 0.4$ in the quiescent state favouring an optically thin emission in contrast to the constantly flat spectra ($\alpha \sim 0.35$) that seems to dominate the outburst phase of GX 339–4 (Tremou et al., in preparation). Although radio emission in quiescence denotes the presence of hard state jets, the wide range of spectral indices that have been previously seen, it is not fully understood (Plotkin et al. 2019) and it may be related with non-canonical jet geometry. Slightly negative spectral index could be seen in the case of a decelerating or a slowly expanding jet, while an inverted spectrum (e.g. A0620−00; Dinçer et al. 2018) could be generated due to the fast expanding parts of the jet (outer regions of the jet).

During our ThunderKAT campaign over the next years, we will be able to constrain the spectral evolution during both the outburst and quiescent state, the latter of which has been poorly understood so far.

ACKNOWLEDGEMENTS

ET and SC acknowledge financial support from the UnivEarthS Labex program of Sorbonne Paris Cité (ANR-10-LABX-0023 and ANR-11-IDEX-0005-02). JCAM-J is the recipient of an Australian Research Council Future Fellowship (FT140101082), funded by the Australian Government. PG acknowledges support from the NRF SARChI program under grant number 111692. PAW acknowledges support from UCT and the NRF. We acknowledge the use of data obtained from the High Energy Astrophysics Science Archive Research Center (HEASARC), provided by NASA's Goddard Space Flight Center. We thank the staff at the South African Radio Astronomy Observatory (SARAO) for scheduling these observations. The MeerKAT telescope is operated by the South African Radio Astronomy Observatory, which is a facility of the National Research Foundation, an agency of the Department of Science and Innovation. This work was carried out in part using facilities and data processing pipelines developed at the Inter-University Institute for Data Intensive Astronomy (IDIA). IDIA is a partnership of the Universities of Cape Town of the Western Cape and of Pretoria. We acknowledge the use of the Nançay Data Center, hosted by the Nançay Radio Observatory (Observatoire de Paris-PSL, CNRS, Université d' Orléans), and also supported by Region Centre-Val de Loire.

REFERENCES

Arnaud K. A., 1996, in Jacoby G. H., Barnes J., eds, ASP Conf. Ser. Vol. 101, Astronomical Data Analysis Software and Systems V. Astron. Soc. Pac., San Francisco, p. 17
Bahramian A. et al., 2018, Radio/X-Ray Correlation Database for X-ray Binaries, https://doi.org/10.5281/zenodo.1252036
Burrows D. N. et al., 2000, in Flanagan K. A., Siegmund O. H., eds, Proc. SPIE Conf. Ser. Vol. 4140, X-Ray and Gamma-Ray Instrumentation for Astronomy XI. SPIE, Bellingham, p. 64
Cadolle Bel M. et al., 2011, A&A, 534, A119
Connors R. M. T. et al., 2017, MNRAS, 466, 4121
Corbel S., Fender R. P., Tzioumis A. K., Nowak M., McIntyre V., Durouchoux P., Sood R., 2000, A&A, 359, 251
Corbel S., Nowak M. A., Fender R. P., Tzioumis A. K., Markoff S., 2003, A&A, 400, 1007
Corbel S., Tomsick J. A., Kaaret P., 2006, ApJ, 636, 971
Corbel S., Koerding E., Kaaret P., 2008, MNRAS, 389, 1697
Corbel S., Coriat M., Brocksopp C., Tzioumis A. K., Fender R. P., Tomsick J. A., Buxton M. M., Bailyn C. D., 2013, MNRAS, 428, 2500
Coriat M. et al., 2011, MNRAS, 414, 677
Dinçer T., Bailyn C. D., Miller-Jones J. C. A., Buxton M., MacDonald R. K. D., 2018, ApJ, 852, 4
Driessen L. N. et al., 2020, MNRAS, 491, 560
Falcke H., Körding E., Markoff S., 2004, A&A, 414, 895
Fender R. P., 2001, MNRAS, 322, 31
Fender R. P., Gallo E., Jonker P. G., 2003, MNRAS, 343, L99
Fender R. P., Gallo E., Russell D., 2010, MNRAS, 406, 1425
Fender R. et al., 2017, preprint (arXiv:1711.04132)
Frater R. H., Brooks J. W., Whiteoak J. B., 1992, J. Electrical Electron. Eng. Aust., 12, 103
Froning C. S. et al., 2011, ApJ, 743, 26
Gallo E., Fender R., Corbel S., 2003a, Astron. Telegram, 196, 1
Gallo E., Fender R. P., Pooley G. G., 2003b, MNRAS, 344, 60
Gallo E., Fender R. P., Hynes R. I., 2005, MNRAS, 356, 1017
Gallo E., Fender R. P., Miller-Jones J. C. A., Merloni A., Jonker P. G., Heinz S., Maccarone T. J., van der Klis M., 2006, MNRAS, 370, 1351
Gallo E., Migliari S., Markoff S., Tomsick J. A., Bailyn C. D., Berta S., Fender R., Miller-Jones J. C. A., 2007, ApJ, 670, 600
Gallo E., Homan J., Jonker P. G., Tomsick J. A., 2008, ApJ, 683, L51
Gallo E., Miller B. P., Fender R., 2012, MNRAS, 423, 590
Gallo E. et al., 2014, MNRAS, 445, 290
Gehrels N. et al., 2004, ApJ, 611, 1005
Hannikainen D. C., Hunstead R. W., Campbell-Wilson D., Sood R. K., 1998, A&A, 337, 460
Hynes R. I., Steeghs D., Casares J., Charles P. A., O'Brien K., 2004, ApJ, 609, 317
Hynes R. I., Bradley C. K., Rupen M., Gallo E., Fender R. P., Casares J., Zurita C., 2009, MNRAS, 399, 2239
Jonas J. L., 2009, IEEE Proc., 97, 1522
Jonker P. G., Bassa C. G., Nelemans G., Juett A. M., Brown E. F., Chakrabarty D., 2006, MNRAS, 368, 1803
King A. R., 2000, MNRAS, 312, L39
Kong A. K. H., McClintock J. E., Garcia M. R., Murray S. S., Barret D., 2002, ApJ, 570, 277
McClintock J. E., Narayan R., Garcia M. R., Orosz J. A., Remillard R. A., Murray S. S., 2003, ApJ, 593, 435
McMullin J. P., Waters B., Schiebel D., Young W., Golap K., 2007, in Shaw R. A., Hill F., Bell D. J., eds, ASP Conf. Ser. Vol. 376, Astronomical Data Analysis Software and Systems XVI. Astron. Soc. Pac., San Francisco, p. 127
Malzac J., 2016, Astron. Nachr., 337, 391

Markoff S., Nowak M. A., 2004, ApJ, 609, 972
Markoff S., Nowak M., Corbel S., Fender R., Falcke H., 2003, A&A, 397, 645
Menou K., Esin A. A., Narayan R., Garcia M. R., Lasota J.-P., McClintock J. E., 1999, ApJ, 520, 276
Merloni A., Heinz S., di Matteo T., 2003, MNRAS, 345, 1057
Miller-Jones J. C. A., Gallo E., Rupen M. P., Mioduszewski A. J., Brisken W., Fender R. P., Jonker P. G., Maccarone T. J., 2008, MNRAS, 388, 1751
Plotkin R. M., Gallo E., Jonker P. G., 2013, ApJ, 773, 59
Plotkin R. M., Gallo E., Markoff S., Homan J., Jonker P. G., Miller-Jones J. C. A., Russell D. M., Drappeau S., 2015, MNRAS, 446, 4098
Plotkin R. M. et al., 2017, ApJ, 834, 104
Plotkin R. M., Miller-Jones J. C. A., Chomiuk L., Strader J., Bruzewski S., Bundas A., Smith K. R., Ruan J. J., 2019, ApJ, 874, 13
Poutanen J., Veledina A., 2014, Space Sci. Rev., 183, 61
Quataert E., Narayan R., 1999, ApJ, 520, 298
Rana V. et al., 2016, ApJ, 821, 103
Remillard R. A., McClintock J. E., 2006, ARA&A, 44, 49
Ribó M. et al., 2017, ApJ, 835, L33
Tasse C. et al., 2018, A&A, 611, A87
Tetarenko B. E. et al., 2016, ApJ, 825, 10
Tremou E., Corbel S., Fender R., Woudt P., Miller-Jones J., Girard J., 2018, Astron. Telegram, 12287, 1
Wu Q. et al., 2016, ApJ, 833, 79
Yuan F., Narayan R., 2014, ARA&A, 52, 529
Zdziarski A. A., Gierliński M., Mikołajewska J., Wardziński G., Smith D. M., Harmon B. A., Kitamoto S., 2004, MNRAS, 351, 791
Zdziarski A. A., Ziółkowski J., Mikołajewska J., 2019, MNRAS, 488, 1026

This paper has been typeset from a TEX/LATEX file prepared by the author.